Contents lists available at ScienceDirect

Chemical Engineering Research and Design

journal homepage: www.elsevier.com/locate/cherd

Mathematical modeling of a composting process in a small-scale tubular bioreactor

Guillermo Vidriales-Escobar[a], Raul Rentería-Tamayo[a], Felipe Alatriste-Mondragón[a], Omar González-Ortega[b,*]

[a] Instituto Potosino de Investigación Científica y Tecnológica, División de Ciencias Ambientales, 2055 Camino a la Presa San José, San Luis Potosí 78216, Mexico

[b] Universidad Autónoma de San Luis Potosí, Facultad de Ciencias Químicas, 6 Manuel Nava, San Luis Potosí 78210, Mexico

ARTICLE INFO

Article history:
Received 25 July 2016
Received in revised form 7 February 2017
Accepted 8 February 2017
Available online 16 February 2017

Keywords:
Mathematical model
Sanitization bioreactor
Bioreactor design
Composting process

ABSTRACT

A mathematical model is presented to describe a composting process occurring in a tubular bioreactor. The mathematical model is based on heat and mass transfer phenomena under the continuum approximation. The bioreactor is divided into two phases: a gas phase and a solid–liquid phase. Between these phases, oxygen and heat are interchanged. In the solid–liquid phase, biomass growth occurs causing a change in substrate concentration as well as a change in temperature due to heat release from microbial activity. Thus the mathematical model is able to describe temperature and oxygen concentration profiles in the gas phase and temperature and biomass and substrate concentration profiles in the solid–liquid phase as a function of time and axial and radial positions. Useful information obtained from the model solution are the highest temperature that can be attained within the bioreactor and the length of high temperature conditions, which are important if sludge sanitization is the purpose of the composting process. Also a theoretical calculation of the logarithmic decimal reduction of *Salmonella* is presented. Using the model, a design analysis was performed to determine the effect of the main design variables in the temperature of the solid–liquid phase and the oxygen concentration in the gas phase.

1. Introduction

Composting represents a series of biochemical reactions in which diverse microorganisms biodegrade organic substrates in a moist, solid state under the presence of oxygen. Four phases are generally accounted for the complete composting process: mesophilic, thermophilic, cooling, and maturation phases. In the mesophilic phase the consumption of easily biodegradable compounds occurs resulting in a mild temperate rise. In the thermophilic phase biodegradation continues by thermophile microorganisms, temperature raises considerably increasing biodegradation of complex substrates with the eventual destruction of most microorganisms. In the cooling phase microorganisms able to biodegrade higher polymers such as starch or cellulose appear. In the maturation phase non-biodegradable compounds appear and the microorganisms are dominated by fungi (Fuchs, 2010; Insam and de Bertoldi, 2007).

The phases of the composting process involve many complex phenomena arising from physicochemical and biological mechanisms. Thus, a proper mathematical description that confidently describes the behavior of the composting process is a difficult task. Once the mathematical model is established, it can be used to determine if a certain bioreactor configuration will be able to behave as expected; mainly in the achievement of high and uniform temperatures. Moreover, it can be used to determine the effect of bioreactor size and process conditions; this is the feasibility of the proposed bioreactor.

In the literature several mathematical models are available to describe a part or the complete composting process. Most of these

* *Corresponding author.*
E-mail addresses: gvidriales@ipicyt.edu.mx (G. Vidriales-Escobar), rrenteria@ipicyt.edu.mx (R. Rentería-Tamayo), falatriste@ipicyt.edu.mx (F. Alatriste-Mondragón), omar.gonzalez@uaslp.mx, ogonzale@email.arizona.edu (O. González-Ortega).
http://dx.doi.org/10.1016/j.cherd.2017.02.006

Nomenclature

a	Internal wall radius (m)
C	Oxygen concentration in solid–liquid phase ($kg\,m^{-3}$)
C_a	Oxygen concentration in gas phase ($kg\,kg^{-1}$)
C_{a0}	Initial oxygen concentration in gas ($kg\,kg^{-1}$)
c_{pa}	Gas phase heat capacity ($J\,kg^{-1}\,K^{-1}$)
c_{pds}	Dried solid (from sludge) heat capacity ($J\,kg^{-1}\,K^{-1}$)
c_{pg}	Grass heat capacity ($J\,kg^{-1}\,K^{-1}$)
c_{pw}	Water heat capacity ($J\,kg^{-1}\,K^{-1}$)
c_{pwc}	Wood chips heat capacity ($J\,kg^{-1}\,K^{-1}$)
D_{eL}	Gas phase axial dispersion coefficient ($m^2\,s^{-1}$)
E_a	Activation energy for growth ($J\,mol^{-1}$)
E_{ab}	Activation energy for death ($J\,mol^{-1}$)
E_{as}	Activation energy for sanitization ($J\,mol^{-1}$)
$h_L\bar{a}$	Volumetric heat transfer coefficient ($W\,m^{-3}\,K^{-1}$)
H	Axial heat transfer coefficient ($W\,m^{-2}\,K^{-1}$)
H_{rx}	Enthalpy of reaction ($J\,kg^{-1}$)
H^{cc}	Henry's law constant for oxygen ($kg\,m^{-3}$)
k_{ds}	Dried solid (from sludge) thermal conductivity ($W\,m^{-1}\,K^{-1}$)
k_{ez}	Gas phase axial thermal conductivity ($W\,m^{-1}\,K^{-1}$)
k_{sl}	Solid–liquid phase thermal conductivity ($W\,m^{-1}\,K^{-1}$)
k_g	Grass thermal conductivity ($W\,m^{-1}\,K^{-1}$)
k_w	Water thermal conductivity ($W\,m^{-1}\,K^{-1}$)
k_{wc}	Wood chips thermal conductivity ($W\,m^{-1}\,K^{-1}$)
k_0	Thermal sanitization coefficient (h^{-1})
K	Oxygen concentration inhibition constant ($kg\,m^{-3}$)
K_c	Half-life kinetic constant ($kg\,kg^{-1}$)
L	Reactor length (m)
n	Final viable pathogen population (–)
n_0	Initial viable pathogen population (–)
r	Radial coordinate (m)
R	Ideal gas constant ($J\,mol^{-1}\,K^{-1}$)
S	Substrate concentration ($kg\,m^{-3}$)
S_o	Initial substrate concentration ($kg\,m^{-3}$)
t	Time coordinate (h^{-1})
T_a	Temperature of the gas phase (°C)
T_{amb}	Ambient air temperature (°C)
T_h	Maximum viable temperature (°C)
T_m	Optimum growth temperature (°C)
T_s	Temperature of the solid–liquid phase (°C)
$T_{s,max}$	Maximum temperature of the solid–liquid phase at the center of the bioreactor (°C)
U	Overall radial heat transfer coefficient ($W\,m^{-2}\,K^{-1}$)
v_i	Interstitial gas velocity ($m\,s^{-1}$)
X	Biomass concentration ($kg\,m^{-3}$)
X_o	Initial biomass concentration ($kg\,m^{-3}$)
$Y_{S/X}$	Substrate to biomass yield ($kg\,kg^{-1}$)
$Y_{O/S}$	Oxygen to substrate yield ($kg\,kg^{-1}$)
$Y_{O/X}$	Oxygen to biomass yield ($kg\,kg^{-1}$)
z	Axial coordinate (m)
α_{ez}	Gas phase axial thermal diffusivity ($m^2\,s^{-1}$)
α_{sl}	Solid liquid phase thermal diffusivity ($m^2\,s^{-1}$)
ε_a	Gas volumetric fraction ($m^{-3}\,m^{-3}$)
ρ_a	Gas phase density ($kg\,m^{-3}$)
ρ_{ds}	Dried solid (from sludge) density ($kg\,m^{-3}$)
ρ_g	Grass density ($kg\,m^{-3}$)
ρ_{sl}	Solid–liquid phase density ($kg\,m^{-3}$)
ρ_{wc}	Wood chips density ($kg\,m^{-3}$)
μ_a	Specific growth rate (s^{-1})
μ_b	Specific death rate (s^{-1})

models rely on the assumption of a perfectly mixed system such that the response variables (temperature, humidity, oxygen concentration, etc.) are considered to only change in time (Mason, 2006; Petric and Mustafic, 2015). This is clearly a major simplification to batch composting systems which ends in having lumped parameters that lose physical meaning. Some other models do not rely on this simplification and describe the response variables as a function of position and time (Nakayama et al., 2007a; Shishido and Seki, 2015). Among these a few works do not introduce a complete description of the models, which limits their application by others looking to describe composting processes. For instance the mathematical model developed by Bongochgetsakul and Ishida (2008) describes the response variables as a function of position and time, but the employed boundary conditions are not clearly established, the composite matrix is treated as a whole with no distinction between temperature of the gas phase and that for the solid–liquid material, and an inhibition factor with two parameters for the specific growth rate is added with no proper explanation for the values selected for these parameters. The inclusion of this inhibition factor will require the measurement of inhibiting degradation products, which is not a simple task in a composting process given the heterogeneity of microorganisms. Moreover, it is not clear why they use the change in Gibb's free energy to characterize the volumetric heat generation when the change in enthalpy (enthalpy of reaction) should be used. In addition, the boundary conditions are not clearly established. In the mathematical model presented by Zambra et al. (2011) to describe the response variables as a function of position and time in compost piles, it is unclear how the biomass and biodegradable substrates participate in the phenomenon description. Moreover the composite pile is treated as a whole with respect to temperature; no distinction is made between temperature in the gas phase and temperature in the solid–liquid phase.

Most of the mathematical modeling, with variations in position, has been applied to describe large rectangular or trapezoidal composting systems with industrial applications (Nakayama et al., 2007a; Zambra et al., 2011). Small-scale bioreactors have been used for composting purposes but their modeling is very limited. This kind of bioreactors is required to optimize the mixture composition to attain composting conditions looking to reduce stabilization times while increasing the high temperature conditions. Composting reactors are, in general, larger in scale; which makes it difficult to run several experiments looking to optimize the mixture composition. Moreover a self-heated bioreactor is desirable such that it behaves more closely to the large-scale systems. Finally, another important feature of small-scale bioreactors is that they can be used to obtain kinetic parameters or parameters associated to heat and mass transfer processes.

In this work, the mathematical description of a composting process is presented along with a design analysis for a small-scale tubular bioreactor. The model is based on mass and heat transport phenomena along with a Contois-type kinetic model as described below; it clearly establishes growth and substrate kinetics, continuity equations for heat and mass, as well as the required initial and boundary conditions.

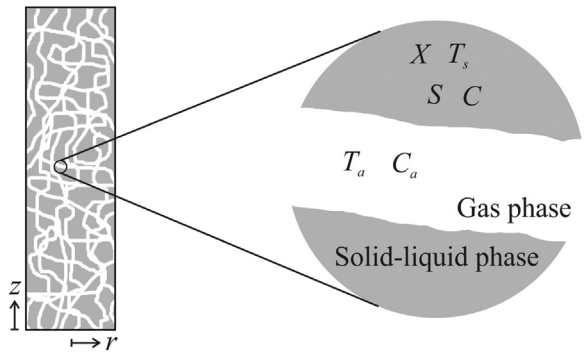

Fig. 1 – Studied bioreactor showing the gas and solid–liquid phases.

2. Materials and methods

2.1. Mathematical model

The mathematical model considers the existence of two phases: a gas phase that supplies the oxygen required for the aerobic degradation of organic matter and a solid–liquid phase where the biomass resides and biodegradation occurs. Heat and oxygen are interchanged by these two phases that are described under the continuum approximation. The bioreactor is isolated to reduce energy losses. Fig. 1 shows a representation of the tubular bioreactor depicting these two phases, moist air is continuously fed at the bottom of the bioreactor. The mathematical model will be able to describe how the biomass and substrate concentrations and the temperature of the solid–liquid phase change in time and positions *r* and z. It will also be able to describe how the oxygen concentration and temperature change in the gas phase. The solid–liquid phase is composed of sludge, water, wood chips, and grass.

2.2. Model assumptions and considerations

For the sake of simplicity, several assumptions and considerations were established: (1) the bioreactor contains a homogeneous mixture of organic material, when running composting processes; the materials being composted were initially mixed such that the composition of the components is as homogeneous as possible (Diaz and Savage, 2007). (2) The thermophysical properties remain constant as well as the reactor porosity, the porosity is known to change during the development of the compost; despite this for the sake of simplicity an average value was used using information reported by Annan and White (1998). (3) The humidity of the material inside the bioreactor is constant; any loss of water from the bioreactor is compensated by the moist air fed at the entrance, the latter is an assumption proposed in this work. It is widely known that moisture content of the composting materials diminishes due to evaporation (Diaz and Savage, 2007), nonetheless if the evaporation is compensated by the water being fed with the gas phase; the moisture content could be kept nearly constant. (4) The reactor is symmetric with respect to the angular coordinate. (5) Oxygen consumption is mainly located at the outermost region of the solid–liquid phase; this condition has been considered by Ge et al. (2015) to model an aerobic composting process. (6) Local equilibrium in the oxygen concentration exists between the gas and the solid–liquid phases as established by Bongochgetsakul and Ishida (2008) to design composting systems. (7) Local equilibrium in temperature exists in the solid–liquid phase. (8) The movement of energy in the *r*-direction is characterized by a constant overall heat transfer coefficient dominated by the thermal resistance of the insulation. (9) The thermophysical properties of the gas phase are considered equal to those of air.

2.3. Growth kinetics

In any composting system, bacteria and fungi participate in the different stages of the process. Despite this, the microorganisms are considered to behave as one and thus their growth kinetics is generally treated as a whole (Kiyasudeen et al., 2016). In the growth kinetics two contributions affect the microorganisms concentration with time, a growth rate and a death rate; both dependent on their concentration (Eq. (1)). Expressions similar to Eq. (1) have been used by others to describe the growth kinetics in composting processes (Hamelers, 2001; Lashermes et al., 2013; Qin et al., 2007; Tremier et al., 2005; Vasiliadou et al., 2015). Both rates are temperature-dependent and the growth rate, in addition, can encompass inhibitory conditions due to substrate concentration.

$$\frac{\partial X}{\partial t} = \mu X - bX \tag{1}$$

For the case of the death coefficient, *b*; the temperature dependence was considered to be Arrhenius-type (Eq. (2)), which is typical for kinetic parameters (Bari et al., 2000; Hamelers, 2004).

$$b = \mu_b \exp\left[-\frac{E_{ab}}{R}\left(\frac{1}{T_s} - \frac{1}{T_h}\right)\right] \tag{2}$$

For the case of substrate inhibition, oxygen and biodegradable substrate concentrations were considered. For the oxygen concentration inhibition a Monod-type (Monod, 1949) relation was used while for the biodegradable substrate concentration a Contois-type (Contois, 1959) was considered (Eq. (3)). The Contois kinetics to describe growth in composting process has been used by Qin et al. (2007) and Nakayama et al. (2007b); and, recently, its theoretical foundation was described for the degradation of insoluble substrates (Wang and Li, 2014). The Monod-type relation to include the effect of oxygen concentration in the growth kinetics is also common (Higgins and Walker, 2003; Lin et al., 2008; Petric and Selimbasic, 2008b; Richard et al., 2006).

$$\mu = \alpha_1 \mu_a \frac{S}{K_c X + S}\frac{C}{K + C} \tag{3}$$

The temperature dependence of the growth rate coefficient, μ, was localized in the α_1 coefficient of Eq. (3) according to Eq. (4) (α_1 is set to 0 when $T_s > T_h$) as reported by Qin et al. (2007) and Nakayama et al. (2007b). Eq. (3) considers that α_1 increases with temperature (which translates into an increase in μ) following an Arrhenius-type behavior until reaching a value of 1.0 when $T_s = T_m$. Further increases in temperature generate a linear decrease in the value of α_1 (microbial activity is restrained due to high temperature) until reaching T_h, this

behavior has been confirmed with experimental data (Rosso et al., 1993; Tremier et al., 2005).

$$\alpha_1 = \begin{cases} \exp\left[-\frac{E_a}{R}\left(\frac{1}{T_s}-\frac{1}{T_m}\right)\right] \\ \frac{T_h - T_s}{T_h - T_m} \end{cases} \quad (4)$$

2.4. Substrate consumption kinetics

The velocity of volatile solids consumption was related to the growth kinetics using a constant substrate to biomass yield coefficient, $Y_{S/X}$, as presented in Eq. (5).

$$\frac{\partial S}{\partial t} = -Y_{S/X}\frac{\partial X}{\partial t} \quad (5)$$

With constant $Y_{S/X}$, Eq. (5) can be integrated to obtain an algebraic relation between substrate and biomass concentration in the solid–liquid phase (Eq. (6)).

$$S = S_0 - Y_{S/X}(X - X_0) \quad (6)$$

2.5. Oxygen transport in the gas phase

A microscopic unsteady-state mass balance on the oxygen in the gas phase within the bioreactor yields Eq. (7).

$$\frac{\partial C_a}{\partial t} + v_i\frac{\partial C_a}{\partial z} = D_{eL}\frac{\partial^2 C_a}{\partial z^2} + \frac{Y_{O/S}}{\varepsilon_a}\frac{\partial S}{\partial t} \quad (7)$$

In Eq. (7), oxygen concentration variations are considered to mainly exist in the z-direction (due to convection and dispersion processes) and the oxygen consumption is related to the substrate consumption through the oxygen to substrate yield coefficient. Also in Eq. (7), the local equilibrium condition for oxygen dissolution in the solid–liquid phase is implicit. Thus, a Henry's law constant is used to relate oxygen concentrations in the gas and solid–liquid phases (Eq. (8)).

$$C = H^{cc}C_a \quad (8)$$

2.6. Energy transport in the gas phase

A microscopic unsteady-state energy balance on the gas phase within the bioreactor yields Eq. (9).

$$\frac{\partial T_a}{\partial t} + v_i\frac{\partial T_a}{\partial z} = \alpha_{ez}\frac{\partial^2 T_a}{\partial z^2} + \alpha_{ez}\frac{1}{r}\frac{\partial}{\partial r}\left(r\frac{\partial T_a}{\partial r}\right) + \frac{h_L\bar{a}}{\varepsilon_a\rho_a c_{pa}}(T_s - T_a) \quad (9)$$

In Eq. (9), radial and axial temperature variations are considered. For the *r*-direction the diffusive heat transfer process was included since the biorreactor can lose energy through its lateral surface that will result in temperature gradients. Also the convective heat transfer process in the *r*-direction was neglected since this process can be envisioned to mainly occur in the z-direction. The last term on the right-hand side of Eq. (9) considers the movement of energy between the gas and solid–liquid phases characterized by a constant volumetric heat transfer coefficient $h_L\bar{a}$.

2.7. Energy transport in the solid–liquid phase

A microscopic unsteady-state energy balance on the solid–liquid phase within the bioreactor yields Eq. (10).

$$\frac{\partial T_s}{\partial t} = \alpha_{sl}\left[\frac{1}{r}\frac{\partial}{\partial r}\left(r\frac{\partial T_s}{\partial r}\right) + \frac{\partial^2 T_s}{\partial z^2}\right] + \frac{H_{rx}}{\rho_{sl}c_{psl}}\frac{\partial S}{\partial t} + \frac{h_L\bar{a}}{\rho_{sl}c_{psl}}(T_a - T_s) \quad (10)$$

Again, in Eq. (10), temperature variations are considered for both coordinates with a uniform solid–liquid thermal diffusivity as well as the movement of energy between phases. Additionally, Eq. (10) shows the energy liberated by the microorganisms due to substrate consumption.

2.8. Initial and boundary conditions

The initial conditions for the mathematical model are:

$$@t = 0, X = X_0, S = S_0, C_a = C_{a0}, T_a = T_{amb}, T_s = T_{amb} \quad (11)$$

The boundary conditions are:

$$@r = 0, \frac{\partial T_a}{\partial r} = \frac{\partial T_s}{\partial r} = 0 \quad (12)$$

$$@r = a, -k_{er}\frac{\partial T_a}{\partial r} = U(T_a - T_{amb}), -k_{sl}\frac{\partial T_s}{\partial r} = U(T_s - T_{amb}) \quad (13)$$

where *U* the overall heat transfer coefficient, is considered constant for both phases and mainly controlled by the thermal resistance of the insulation.

$$@z = 0, -k_{ez}\frac{\partial T_a}{\partial z} = v_i\rho_a c_{pa}(T_{amb} - T_a), T_s = T_{amb} \quad (14)$$

$$@z = L v_i, \rho_a c_{pa}T_a - k_{ez}\frac{\partial T_a}{\partial z} = h(T_a - T_{amb}), -k_{sl}\frac{\partial T_s}{\partial z} = h(T_s - T_{amb}) \quad (15)$$

The boundary condition at $z = L$ for T_a considers a convective heat transfer coefficient, *h*, to describe the energy transport beyond the biorreactor as a simplification.

2.9. Dimensionless mathematical model

The following dimensionless variables were defined

$$\bar{X} = \frac{X}{X_0}, \bar{S} = \frac{S}{S_0}, \bar{C}_a = \frac{C_a}{C_{a0}}, \bar{T}_a = \frac{T_a}{T_{amb}}, \bar{T}_s = \frac{T_s}{T_{amb}}, \bar{t} = \frac{t}{L/v_i}, \bar{z} = \frac{z}{L}, \bar{r} = \frac{r}{a} \quad (16)$$

Where the gas phase residence time is used to scale the time coordinate. Using these dimensionless variables the mathematical model is as follows:

$$\frac{\partial \bar{X}}{\partial \bar{t}} = \frac{Da_g\alpha_1\bar{X}\bar{S}\bar{C}_a}{\left(d\bar{X} + \bar{S}\right)\left(c + \bar{C}_a\right)} - Da_d\alpha_2\bar{X} \quad (17)$$

$$\bar{S} = 1 - e\left(\bar{X} - 1\right) \quad (18)$$

$$\frac{\partial \bar{C}_a}{\partial \bar{t}} + \frac{\partial \bar{C}_a}{\partial \bar{z}} = \frac{1}{Pe}\frac{\partial^2 \bar{C}_a}{\partial \bar{z}^2} - f\frac{\partial \bar{X}}{\partial \bar{t}} \quad (19)$$

$$\frac{\partial \bar{T}_a}{\partial \bar{t}} + \frac{\partial \bar{T}_a}{\partial \bar{z}} = \frac{1}{Pe_z}\frac{\partial^2 \bar{T}_a}{\partial \bar{z}^2} + \frac{1}{Pe_r}\frac{1}{\bar{r}}\frac{\partial}{\partial \bar{r}}\left(\bar{r}\frac{\partial \bar{T}_a}{\partial \bar{r}}\right) + St_{sa}\left(\bar{T}_s - \bar{T}_a\right) \quad (20)$$

Table 1 – Input data for the mathematical model.

Parameter	Value	Units	Reference
a	0.127	m	
C_{a0}	0.2275	kg kg^{-1}	Calculated
c_{pa}	1007	J kg^{-1} K^{-1}	
c_{pds}	1020	J kg^{-1} K^{-1}	Ahn et al. (2009)
c_{pg}	1520	J kg^{-1} K^{-1}	Ahn et al. (2009)
c_{psl}	2122	J kg^{-1} K^{-1}	Calculated
c_{pw}	4188	J kg^{-1} K^{-1}	
c_{pwc}	1760	J kg^{-1} K^{-1}	Ahn et al. (2009)
D_{eL}	2.14×10^{-6}	m^2 s^{-1}	Assumed
E_a	41,250	J mol^{-1}	Calculated
E_{ab}	52,000	J mol^{-1}	Assumed
h	5	W m^{-2} K^{-1}	Assumed
$h_L\bar{a}$	400	W m^{-3} K^{-1}	Calculated
H_{rx}	1.99×10^7	J kg^{-1}	Weppen (2001)
H^{cc}	0.029	kg m^{-3}	Sander (2015)
k_{ds}	0.12	W m^{-1} K^{-1}	Ahn et al. (2009)
k_{ez}	0.15	W m^{-1} K^{-1}	Calculated
k_{ez}	0.13	W m^{-1} K^{-1}	Assumed
k_{sl}	0.21	W m^{-1} K^{-1}	Calculated
k_g	0.05	W m^{-1} K^{-1}	Ahn et al. (2009)
k_w	0.6	W m^{-1} K^{-1}	
k_{wc}	0.06	W m^{-1} K^{-1}	Ahn et al. (2009)
K	0.0015	kg m^{-3}	Assumed
K_c	10	–	Nakayama et al. (2007b)
L	2.54	m	
R	8.314	J mol^{-1} K^{-1}	
S_o	18	kg m^{-3}	Assumed
T_{amb}	25	°C	
T_h	80	°C	Nakayama et al. (2007b)
T_m	60	°C	Nakayama et al. (2007b)
U	2.2	W m^{-2} K^{-1}	Assumed
v_i	4.13×10^{-4}	m s^{-1}	Kulcu and Yaldiz (2004)
X_o	2	kg m^{-3}	Assumed
$Y_{S/X}$	2	kg kg^{-1}	Hamelers (2004)
$Y_{O/S}$	0.7	kg kg^{-1}	Petric and Selimbasic (2008b)
$Y_{O/X}$	$Y_{S/X}Y_{O/X}$		
α_{ez}	$k_{ez}/\rho_a c_{pa}$	m^2 s^{-1}	
α_{sl}	$k_{sl}/\rho_{sl} c_{psl}$	m^2 s^{-1}	
ε_a	0.41	–	Calculated
ρ_a	1.2	kg m^{-3}	
ρ_{ds}	749.6	kg m^{-3}	Ahn et al. (2009)
ρ_g	216	kg m^{-3}	Ahn et al. (2009)
ρ_{sl}	526	kg m^{-3}	Calculated
ρ_{wc}	150	kg m^{-3}	Ahn et al. (2009)
μ_a	5.5×10^{-5}	s^{-1}	Calculated
μ_b	1.0×10^{-5}	s^{-1}	Assumed

$$\frac{\partial \overline{T}_s}{\partial \bar{t}} = \frac{1}{Pe_{sr}}\frac{1}{\bar{r}}\frac{\partial}{\partial \bar{r}}\left(\bar{r}\frac{\partial \overline{T}_s}{\partial \bar{r}}\right) + \frac{1}{Pe_{sz}}\frac{\partial^2 \overline{T}_s}{\partial \bar{z}^2} - g\frac{\partial \overline{X}}{\partial \bar{t}} + St_{as}\left(\overline{T}_a - \overline{T}_s\right) \quad (21)$$

where several dimensionless numbers appear as parameters of the model, these are defined as:

$$Da_g = \frac{L}{v_i}\mu_a,\ Da_d = \frac{L}{v_i}\mu_b,\ c = \frac{K}{H^{cc}C_{a0}},\ d = K_c\frac{X_0}{S_0},$$
$$e = Y_{S/X}\frac{X_0}{S_0},\ Pe = \frac{v_i L}{D_{eL}},\ f = \frac{Y_{O/X}X_0}{\varepsilon_a C_{a0}},\ Pe_z = \frac{v_i L}{\alpha_{ez}},$$
$$Pe_r = \frac{v_i a^2}{\alpha_{er}L},\ St_{sa} = \frac{h_L\bar{a}L}{\varepsilon_a\rho_a c_{pa}v_i},\ Pe_{sr} = \frac{v_i a^2}{\alpha_{sl}L},\ Pe_{sz} = \frac{v_i L}{\alpha_{sl}},$$
$$g = \frac{Y_{S/X}H_{rx}S_0}{\rho_{sl}c_{psl}T_{amb}},\ St_{as} = \frac{h_L\bar{a}L}{\rho_{sl}c_{psl}v_i} \quad (22)$$

The initial and boundary conditions change to

$$@\bar{t} = 0,\ \overline{X} = 1,\ \overline{S} = 1,\ \overline{C}_a = 1,\ \overline{T}_a = 1,\ \overline{T}_s = 1 \quad (23)$$

$$@\bar{r} = 0,\ \frac{\partial \overline{T}_a}{\partial \bar{r}} = \frac{\partial \overline{T}_s}{\partial \bar{r}} = 0 \quad (24)$$

$$@\bar{r} = 1,\ -\frac{1}{Bi_r}\frac{\partial \overline{T}_a}{\partial \bar{r}} = \overline{T}_a - 1,\ -\frac{1}{Bi_{sr}}\frac{\partial \overline{T}_s}{\partial \bar{r}} = \overline{T}_s - 1 \quad (25)$$

$$@\bar{z} = 0\ \ -\frac{1}{Pe_z}\frac{\partial \overline{T}_a}{\partial \bar{z}} = 1 - \overline{T}_a,\ \overline{T}_s = 1 \quad (26)$$

$$@\bar{z} = 1,\ \overline{T}_a - \frac{1}{Pe_z}\frac{\partial \overline{T}_a}{\partial \bar{z}} = St\left(\overline{T}_a - 1\right),\ -\frac{1}{Bi_{sz}}\frac{\partial \overline{T}_s}{\partial \bar{z}} = \overline{T}_s - 1 \quad (27)$$

where

$$Bi_r = \frac{Ua}{k_{er}},\ Bi_{sr} = \frac{Ua}{k_{sl}},\ Bi_{sz} = \frac{hL}{k_{sl}},\ St = \frac{h}{\rho_a c_{pa} v_i} \quad (28)$$

2.10. Input data

Table 1 shows the input data employed to solve the proposed mathematical model, references are provided for data directly used. Data stated as calculated are, in general, average values gathered from the literature or results from proper correlations as described below. Data stated as assumed represent values not directly reported in the literature, how these values were set is also described below.

For initial calculations the ratio between the length of the reactor, L, and its radius was set to 20; with a set to 0.127 m. For the initial oxygen concentration calculation, air saturated with water at 25 °C was considered. The composition of oxygen in dry air is 0.232 kg kg^{-1} while the humidity of saturated air is 0.020 kg kg^{-1}, thus the required oxygen concentration is 0.232/1.02 = 0.2275 kg/kg^{-1}. The heat capacity of the solid–liquid phase was estimated as the average of the heat capacities of its four components, the same was performed for the thermal conductivity and density. For these calculations the data (also included in Table 1) provided by Ahn et al. (2009) were used. For instance c_{psl} was calculated as (1020 + 1520 + 4188 + 1760)/4 = 2122 J kg^{-1} K^{-1}.

The axial heat transfer coefficient, h, was considered higher than the value estimated using a correlation for natural convection from a horizontal disk (Sahraoui et al., 1990) to account for an additional heat transfer due to air movement. This correlation predicts a value of 1.9 W m^{-2} K^{-1} for a surface temperature of 27 °C while a value of 3.4 W m^{-2} K^{-1} is predicted for 60 °C, which was the highest expected temperature.

The Henry's law constant, in Table 1, is an average of values at 25 and 60 °C according to Sander (2015) for the sake of simplicity; in the model a constant (H^{cp}) of 1.3 × 10^{-5} mol m^{-3} Pa^{-1} was used considering a change in dln H^{cp}/d(1/T_s) = 1500 K to account for oxygen solubility changes. To relate H^{cp} with H^{cc} the oxygen density was considered as 1.105 kg m^{-3} (H^{cc} = 1.105$H^{cp}RT_s$).

The gas phase axial dispersion coefficient was considered as one order of magnitude smaller than the oxygen diffusivity in saturated air (2.14 × 10^{-5} m^2 s^{-1}) (Cornell Waste Management Institute, 1996) since the studied gas phase velocities imply small (<1.0) Peclet (Pe_m) numbers (Pe_m is defined as dv_i/D_{eL} where d is the particle diameter, which was set to 2 cm for this calculation and for the estimation of $h_L\tilde{a}$). Thus, according to Delgado (2007), D_{eL} is smaller than the oxygen diffusivity in saturated air under the studied conditions.

The gas phase volumetric fraction was an average of values reported by Annan and White (1998), with this fraction and the thermal conductivity of the solid–liquid phase; the effective thermal conductivity of quiescent air was calculated using the correlation by Krupiczka (1967). This value was assigned to the gas phase axial thermal conductivity, k_{ez}, while k_{er} was considered slightly smaller. The oxygen concentration inhibition constant was set to 0.0015 kg m^{-3}, which has the same order of magnitude of the product $C_{a0}H^{cc}$ such that the value for c ($K/C_{a0}{\cdot}H^{cc}$) still accounts for inhibition by oxygen concentration. The volumetric heat transfer coefficient was set to 400 W m^{-3} K^{-1} since the value of h_L was calculated as 2.4 W m^{-2} K^{-1} (Bergman et al., 2011) for a particle diameter of 2 cm with specific area ($6(1-\varepsilon_a)/d$) of 177 m^2 m^{-3}.

The substrate to mass yield was set to 2.0 (Hamelers, 2004; Nakayama et al., 2007a; Qin et al., 2007) and the half-life kinetic constant, K_c, to 10 since according to Nakayama et al. (2007b) the ratio $K_c/Y_{S/X}$ = 4 ∼ 20. For the gas phase velocity, a value of 0.4 L min^{-1} kg^{-1} was used (Kulcu and Yaldiz, 2004); which results in 4.13 × 10^{-4} m s^{-1} for the interstitial velocity under the initial input data. A value of 0.7 kg kg^{-1} was used for the oxygen to substrate yield according to Petric and Selimbasic (2008b). The activation energy for growth was an average of values reported by Nakayama et al. (29,000 J mol^{-1}) (2007a) and McKinley and Vestal (58,600 J mol^{-1}) (1984). For the case of the activation energy for death a value of 52,000 J mol^{-1} was used since it has to be larger than the value for growth. The specific growth rate was set to 5.5 × 10^{-5} s^{-1} which is an average of values reported by Sole-Mauri et al. (3.89 × 10^{-5} s^{-1}) (2007) and Hamelers (7.0 × 10^{-5} s^{-1}) (2004) for composting processes. The specific death rate was selected such that $\alpha_1\,\mu_a > b$ for any temperature, thus μ_b was assumed as 1.0 × 10^{-5} s^{-1}. Since it is considered that the bioreactor is isolated to reduce energy losses in the r-direction, the overall radial heat transfer coefficient was considered as being lower than the heat transfer coefficient for natural convection at a surface temperature of 60 °C calculated using the correlation of Churchill and Chu (4.3 W m^{-1} K^{-1}) (1975).

2.11. Model solution

The dimensionless mathematical model, Eqs. (17)–(28), was solved using the method of lines (Davis, 1984). The axial and radial coordinates were discretized using 2nd order finite differences while ODE15s from Matlab® was used for integration in time of the system of ordinary differential equations. 21 nodes were used in the r-direction while 49 were used in the z-direction. The number of nodes was previously determined to be sufficient to obtain non-oscillating, non-changing solutions.

2.12. Sanitization

Once the mathematical model is solved, the temperature profile of the solid–liquid phase, where the microorganisms exist; will be known and a theoretical analysis can be performed for the desired sanitization. For this a classical first order decay model was considered with *Salmonella* as the model pathogen, the logarithmic decimal reduction was estimated using Eq. (29) (Haug, 1993).

$$\log_{10}\left(\frac{n}{n_0}\right) = -\frac{1}{2.303}\int_0^t k_0 \exp\left(-\frac{E_{as}}{RT_s}\right) \tag{29}$$

This logarithmic decimal reduction was calculated for each point (discretization node) within the bioreactor. Afterwards, the percentage of nodes where the reduction stayed below 10 was estimated. For calculations the values reported by Gea et al. (2007) were used, k_0 = 5.058 × 10^{68} h^{-1} and E_{as} = 430,115 J mol^{-1}.

3. Results and discussion

3.1. Model simulation results

The mathematical model is able to predict concentration profiles for biomass, substrate, and oxygen concentrations in the solid–liquid phase as well as temperature profiles for both phases. Fig. 2 shows temperature profiles for the solid–liquid phase as a function of time. This temperature profile is the most important prediction of the model since it establishes

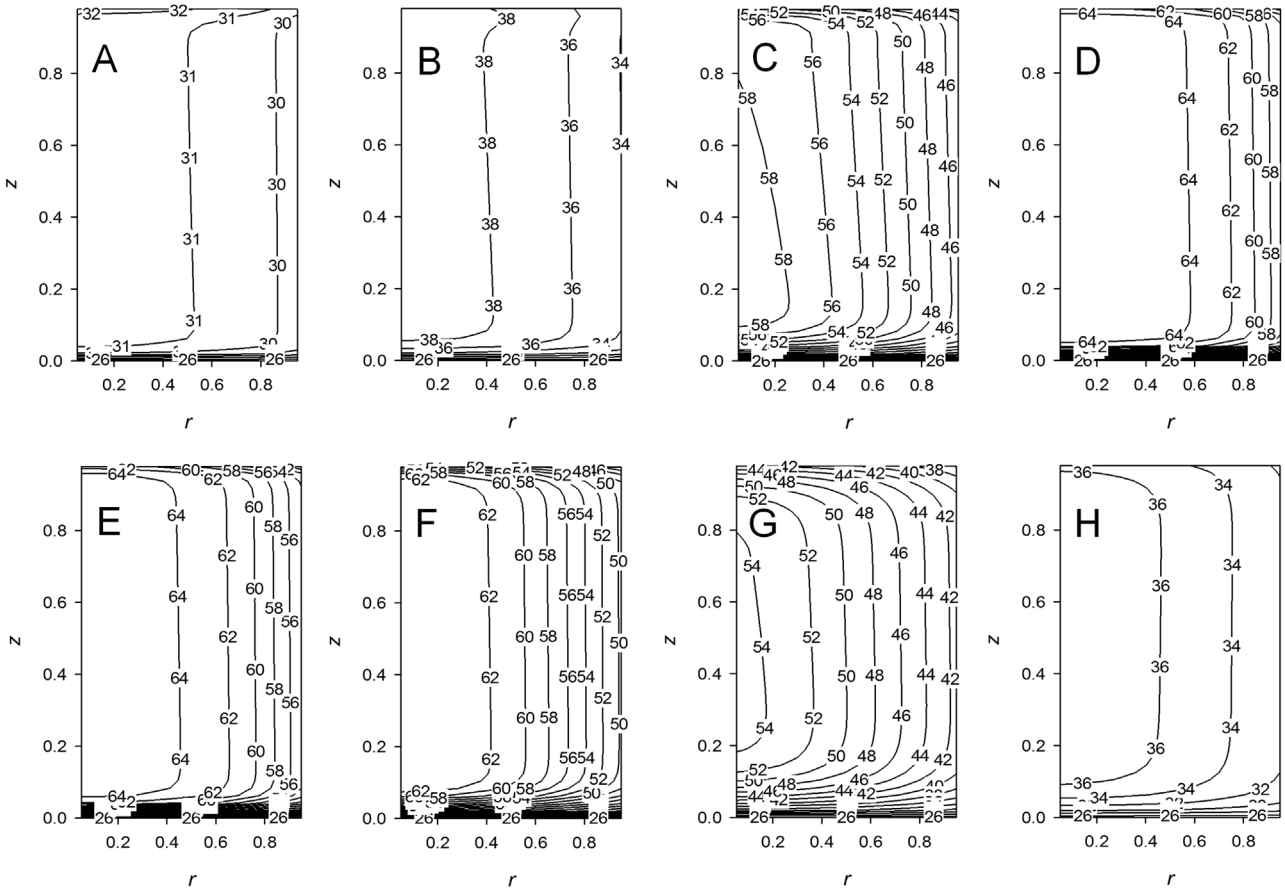

Fig. 2 – Solid–liquid phase temperature profiles for different periods. (A) 2.5 h, (B) 5 h, (C) 10 h, (D) 20 h, (E) 40 h, (F) 80 h, (G) 140 h, (H) 250 h.

Table 2 – Maximum temperature and length of high temperature conditions.

$T_{s.max}$ [°C]	LHT [h]	Reference
66	145	Shishido and Seki (2015)
65	130	Qin et al. (2007)
60	120	Bari et al. (2000)
65	89	Lin et al. (2008)
64	96	Petric and Selimbasic (2008b)
67	170	Sole-Mauri et al. (2007)
64	156	Briski et al. (2003)
68	132	Ge et al. (2015)
63	86	Petric and Selimbasic (2008a)
59	170	VanderGheynst et al. (1997)
66	144	This work

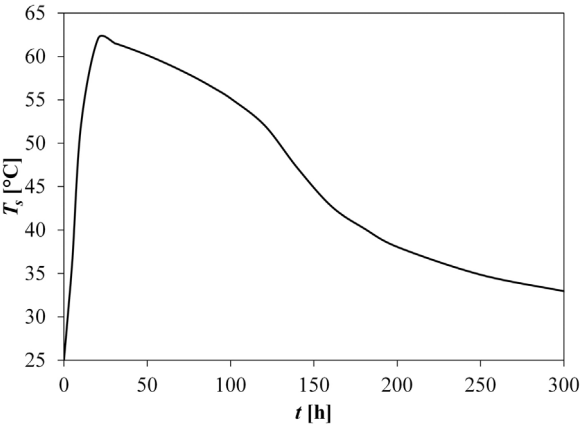

Fig. 3 – Solid–liquid phase average temperature.

the maximum temperature that can be attained in the bioreactor as well as the length of high temperature conditions. This information is critical if sludge sanitization is pursued.

According to Fig. 2, the temperature of the solid–liquid phase rapidly increases resulting in the development of a highest temperature region close to the bioreactor entrance; the highest temperature reached within the reactor was 65.6 °C at 17 h localized at the center of the bioreactor and 0.5 m in the z-direction. Analyzing this high temperature point within the reactor, the length of high temperature (LHT) conditions (temperature above 50 °C) lasts for 144 h. It is interesting to compare experimental data from the literature for composting processes. Table 2 shows the highest temperature achieved within the bioreactor, from literature, as well as the length of high temperature conditions. From the data shown in Table 2, it is clear that the proposed mathematical model behaves as expected with respect to the temperature within the bioreactor when composting processes are occurring.

Fig. 3 shows the average temperature (for the whole bioreactor) of the solid–liquid phase. This average temperature is higher than 50 °C for a period of 110 h and the highest standard deviation for the same period is in the 6.2–7.5 °C range. Temperature uniformity within the bioreactor is a desired condition to avoid low temperature regions where pathogens could continue to grow avoiding a proper sanitization of the material in the bioreactor.

The temperature profile behavior shown in Fig. 3 is representative for each point within the bioreactor; the temperature in the solid–liquid phase rapidly increases at the beginning of the simulation reaching average temperatures greater than

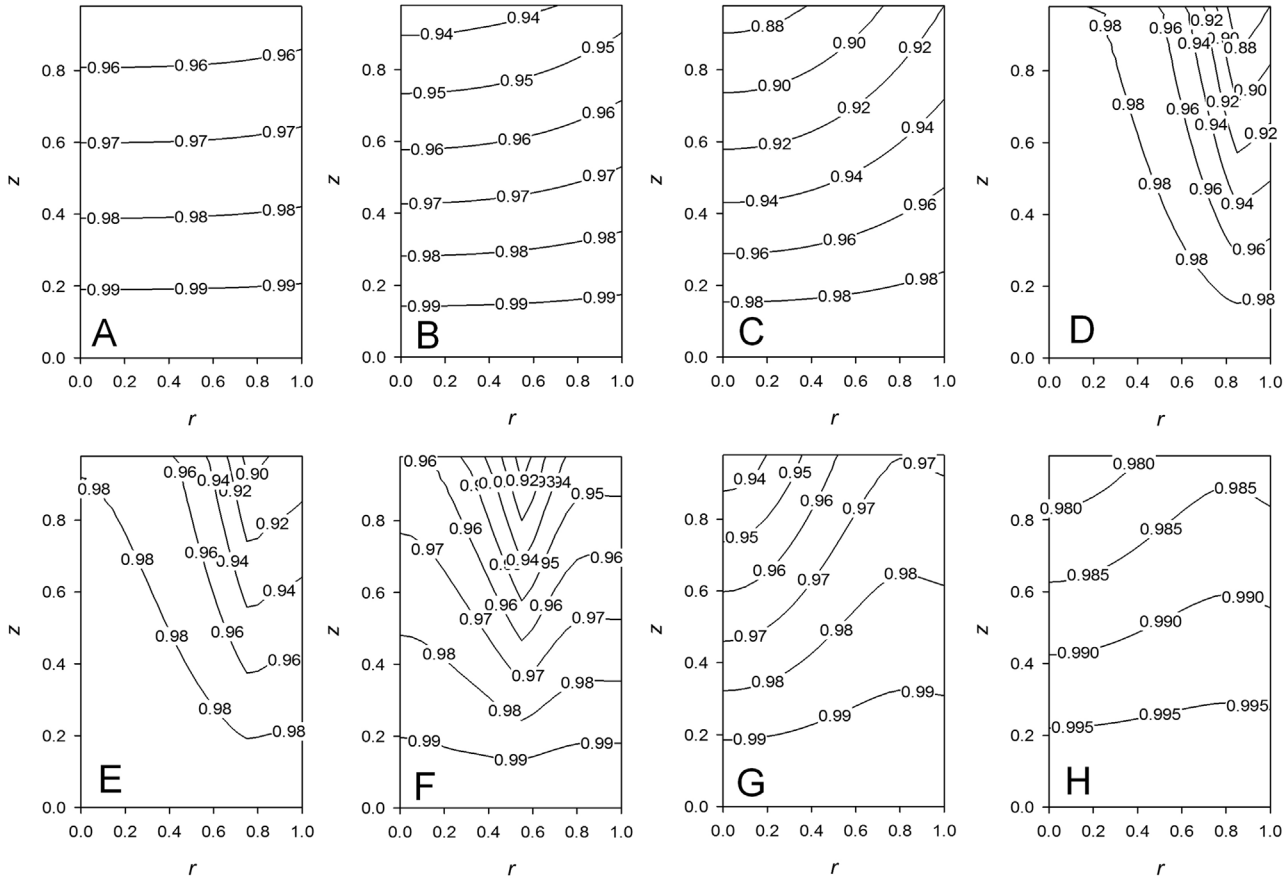

Fig. 4 – Gas phase dimensionless oxygen concentration profiles for different periods. (A) 2.5 h, (B) 5 h, (C) 10 h, (D) 20 h, (E) 40 h, (F) 80 h, (G) 140 h, (H) 250 h.

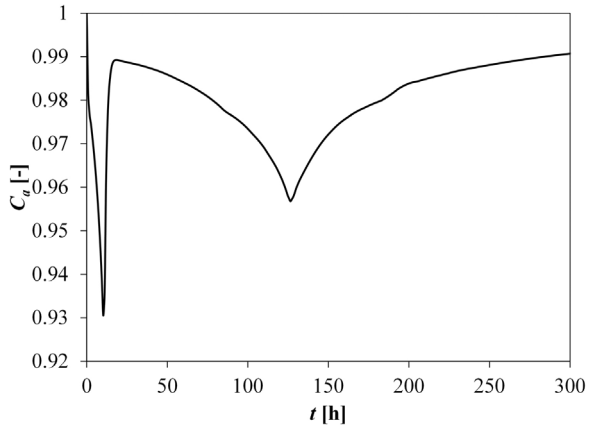

Fig. 5 – Dimensionless oxygen concentration in the gas phase at the center of the bioreactor.

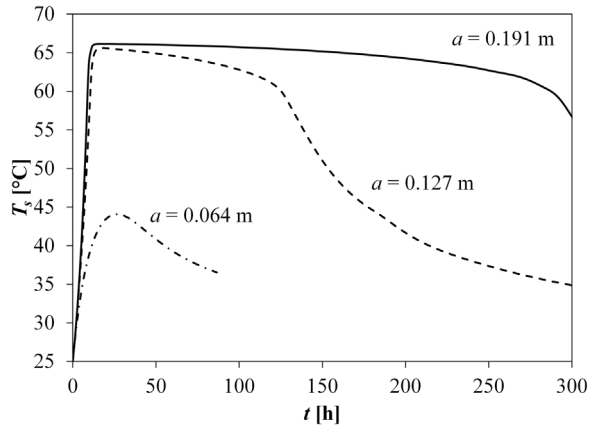

Fig. 6 – Solid–liquid phase temperature at the center of the bioreactor as a function of changes in *a*.

60 °C after 17 h. After this time, the temperature increases slightly since the optimum growth temperature was fixed at 60 °C; this promotes a decrease in the maximum growth rate of the microorganisms. When the temperature decreases below 60 °C, the growth is once again favored. The temperature will continue decreasing since the amount of heat released by the microorganisms is less than the amount lost to the ambient air. The behavior shown in Fig. 3 is typical for composting processes.

Fig. 4 shows the predicted oxygen concentration profiles in the gas phase within the bioreactor. Since oxygen is being fed at z = 0, the highest oxygen concentration always exists close to this position. At the beginning of the simulation (t < 10 h), the oxygen concentration is being reduced with a higher consumption close to z = L. Once the average temperature rises above 60 °C (which happens after 17 h), the oxygen concentration profiles notably change since the biomass growth is reduced. Within the bioreactor, regions where the temperature has not reached 60 °C exist showing higher oxygen consumption. Once the solid–liquid phase cools to values below 60 °C, oxygen consumption increases again but at slower rates. Fig. 5 shows the oxygen concentration profiles in the gas phase at the center of the bioreactor. Here, it is more evident that at the beginning of the simulation, higher biomass growth rate occurs resulting in a rapid drop of oxygen concentration. Afterwards the oxygen concentration starts to increase when temperatures above 60 °C are reached, when the bioreactor cools below 60 °C; the biomass growth rate increases again

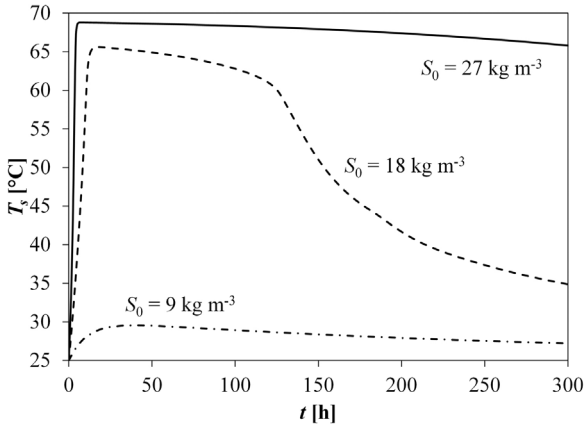

Fig. 7 – Solid–liquid phase temperature at the center of the bioreactor as a function of S_0.

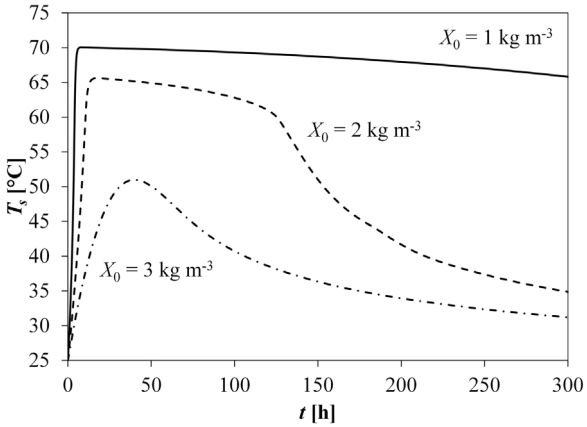

Fig. 8 – Solid–liquid phase temperature at the center of the bioreactor as a function of X_0.

dropping once again the oxygen concentration but at a slower rate. When the biomass growth rate decreases due to substrate availability, the oxygen concentration starts to rise. The behavior shown in Fig. 5, in which two regions of dropping oxygen concentrations appear, has been previously reported by VanderGheynst et al. (1997) and Mohee et al. (1998). Shishido and Seki (2015) also show oxygen concentration profiles with analogous behavior and their proposed mathematical model also behaves similarly.

3.2. *The design process*

The main aspect of any mathematical model intended to describe a phenomenon is helping the design process. For the case of the bioreactor a study can be performed using the simulation results to determine the behavior, mainly of the solid–liquid phase temperature profile, when the design variables are changed. For a fixed reactor length it is desirable to know how changes in the bioreactor radius or the air velocity affect the temperature profiles. Moreover the model allows changing the initial substrate and biomass concentrations predicting their importance in the sanitization process.

Fig. 6 shows temperature profiles of the solid–liquid phase as a function of the bioreactor radius for a fixed air volumetric flow rate (75 L h^{-1}). According to Fig. 6, high temperature conditions are favored if the radius increases. Since the air volumetric flow rate entering the bioreactor is fixed, an increase in the bioreactor radius will decrease the air interstitial velocity. The changes in the temperature profiles of the solid–liquid phase are mainly promoted by an increase in the Da $_g$ number that will favor the growth of the microorganisms releasing a higher amount of heat from biochemical reactions, despite the fact that increasing the bioreactor radius increases the area for heat transfer to the ambient air. Moreover the Pe $_{sr}$ number remains unchanged since the product $a^2 v_i$ is constant. The simulation run using data from Table 1 estimated that 4.5% of the nodes used to discretize the mathematical model had a logarithm decimal reduction below 10, this percentage increased to 100% for a smaller bioreactor and decreased to 2.7% for the larger one. The coldest nodes, without considering the nodes located at the entrance of the bioreactor, are localized near the bioreactor surface.

Changes in the length of the bioreactor did not modify the solid–liquid phase temperature profiles since Pe $_{sz}$ » Pe $_{sr}$ > 1.0, moreover the balance between growth and death is unchanged since Da $_g$/Da $_d$ is constant and equal to 5.5. This also implies that the oxygen concentration in the solid–liquid phase is not a limiting factor. Under the studied conditions, changes in v_i also did not modify the solid–liquid phase temperature profiles since the changes in the model are equivalent to changes induced by the variation in L. When the oxygen concentration in the solid–liquid phase becomes a limiting factor, changes in the solid–liquid phase temperature profiles will be expected.

When loading the material into a bioreactor for composting process, it is possible to change the initial amount of sludge and the initial amount of substrate for biodegradation. Thus the behavior of the model was analyzed for variations in S_0 and X_0. Figs. 7 and 8 show the predicted solid–liquid phase temperature profiles for changes in S_0 and X_0, respectively. An increase in the initial substrate concentration favors the highest temperature than can be reached and the length of high temperature conditions since more substrate is available for biodegradation. From Fig. 7, it is clear that the model prediction is highly sensitive to the initial substrate concentration. Increasing the initial substrate concentration increases the g number and reduces the d number; the latter will promote higher changes in biomass concentration while the former, in conjunction with the latter, will promote higher changes in the solid–liquid phase temperature. According to Eq. (29), 100% of the nodes within the bioreactor showed logarithm decimal reduction below 10 for the lowest initial concentration of substrate while significant reduction (2.0%) was achieved for the highest initial substrate concentration.

For the case of changes in the initial biomass concentration, Fig. 8 shows that increasing this concentration results in lower maximum temperatures and shorter periods of high temperature conditions. Since for this simulation the initial substrate concentration is fixed to 18 kg m^{-3}, an increase in initial biomass concentration will not favor the composting process if the substrate concentration is limiting the development of the sanitization. This is the case for the studied conditions, thus the ratio S_0/X_0 is important for design considerations. If the purpose of the bioreactor is to sanitize sludge, a compromise emerges since it is desirable to treat as much sludge as possible but without obtaining low temperature conditions. With respect to sanitization, even though; for the case of X_0 = 3 kg m^{-3}, the temperature at the center of the reached 50 °C; the logarithmic decimal reduction was below 10 for 98% of the discretization nodes. This value decreased to 2.0% when the smallest initial concentration of biomass was considered.

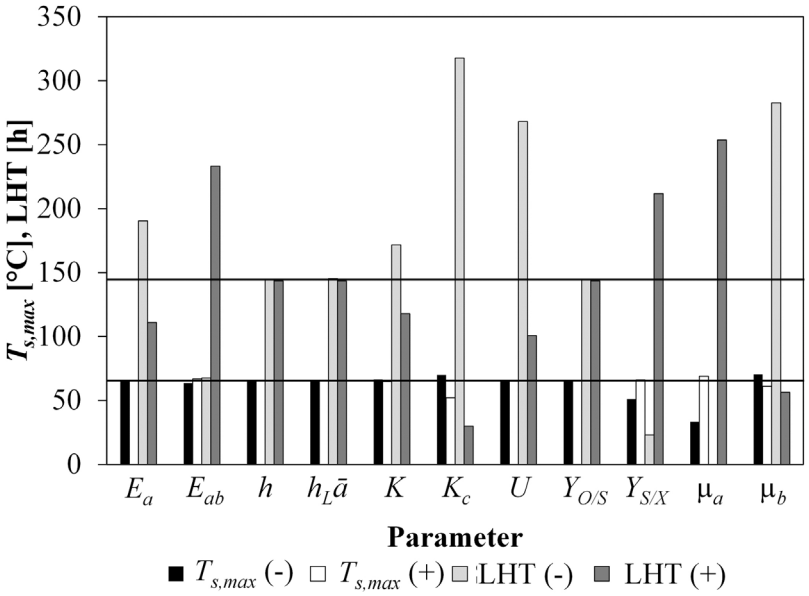

Fig. 9 – Effect of the mathematical model parameters on $T_{s,max}$ and LHT.

Table 3 – F-test for the sensitivity analysis.

Parameter	F	
	T_s	C_a
E_a	70.1	76.1
E_{ab}	282.2	212.2
h	0.0	0.0
$h_L\bar{a}$	0.0	0.0
K	18.4	13.1
K_c	897.5	211.3
U	182.3	5.7
$Y_{O/S}$	0.0	289.6
$Y_{S/X}$	271.2	144.5
μ_a	871.2	433.3
μ_b	454.2	212.4

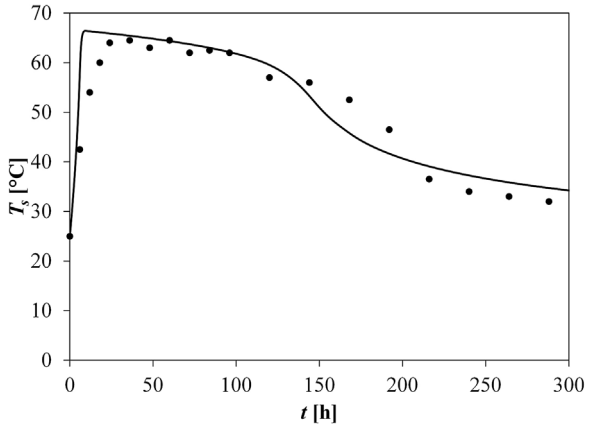

Fig. 10 – Comparison of temperature profiles predicted by the model and experimental data reported by Briski et al. (2003).

3.3. *Sensitivity analysis*

Aside from the design variables, several parameters exist in the model and a sensitivity analysis was carried out to determine the magnitude of their effect in the temperature of the solid–liquid phase and the oxygen concentration of the gas phase. For this, each parameter was independently changed by +50% and −50% of its original value (except for E_a and E_{ab} that were changed ±20% to avoid a situation in which death prevails over growth) and an *F*-test was performed on the profiles at the center of the bioreactor. The results are shown in Table 3 with $F_{crit} = 3.0$, additionally Fig. 9 shows the maximum temperatures ($T_{s,max}$) and the duration length of temperatures above 50 °C (LHT). For the simulation using the original values for the parameters (Table 1), $T_{s,max}$ is equal to 65.6 °C while LHT is equal to 144.4 h.

Both the solid–liquid phase temperature and the oxygen concentration in the gas phase resulted insensitive to changes in h and $h_L\bar{a}$. Both are coefficients associated to heat transfer processes, the first is used to estimate the energy transport at the end of the bioreactor while the second is used to estimate the energy transport between the solid–liquid and gas phases. The value of h affects the Bi $_{sz}$ and St numbers, nonetheless their values are always greater than 10; which implies that the temperature rapidly decreases approaching T_{amb} at the exit of the bioreactor.

Also the temperature of the solid–liquid phase was insensitive to changes in $Y_{O/S}$. In most of the changes in value of the studied parameters, $T_{s,max}$ remains at values higher than 60 °C; nonetheless the duration length of high temperature conditions is greatly modified.

From all the parameters than influence the mathematical model response, the parameter K affects the less. This situation can be associated to the oxygen concentration profiles that imply that the oxygen concentration in the solid–liquid phase does not fall considerably upon oxygen consumption by the biomass. Thus high aeration conditions exist under the studied conditions.

A change in the value of K_c greatly influences the value of LHT. A reduction in its value increases the value of LHT, this can be associated to the relation between K_c and the substrate. According to Wang and Li (2014) K_c is related to how much the substrate surface is covered by microorganisms. A high coverage represents a smaller value of K_c and thus an increase in LHT is produced.

The case of the overall radial heat transfer coefficient, U, needs to be considered as a design variable related to the isolation used for the bioreactor. Its value will be dominated by the thermal resistance of the material used for the isolation, thus an increase in U will be related to a decrease in the isolation thickness. According to Fig. 9 a change in its value did not change, significantly, the maximum temperature attained but this not holds true for the value of LHT, which significantly increases with a reduction in the value of U. This behavior can also be associated to the value of Bi_r and Bi_{sr} that for any studied change remained close to 1.0.

The specific growth and death rates greatly influence the temperature profile. The observed results are expected, a high value of μ_a with a small value of μ_b favored biomass growth increasing the value of LHT. The activation energies for growth, E_a, and death, E_{ab}, also changed the model output as expected. A small value of E_a combined with a large value of E_{ab} favored biomass growth.

3.4. *Model prediction comparison with literature data*

The proposed mathematical model was tested looking to describe composting results from the literature. For this the experimental data reported by Briski et al. (2003) were used. In their article Briski et al. used a 25 L column reactor to perform composting processes. The reactor had an internal diameter of 0.19 m ($a = 0.095$ m), a length of 0.85 m, and it was insulated. The employed airflow superficial velocity was set to $4 \times 10^{-3}\,m\,s^{-1}$. The remaining parameters were unchanged except for S_0 and U, which were set to $23\,kg\,m^{-3}$ and $2.4\,W\,m^{-2}\,K^{-1}$; respectively. Fig. 9 shows the comparison between the experimental data and the predicted values for the solid–liquid phase temperature at the middle of the reactor, it can be seen that the model shows resemblance to the behavior of the experimental data. Despite this, additional efforts must be conducted such that the model is able to optimize the values for the most important parameters according to the sensitivity analysis (Fig. 10).

4. Conclusions

A mathematical model based in the continuum approximation to describe heat and mass transport phenomena occurring in a tubular bioreactor during a composting process was developed. As constitutive equation, a Contois-type kinetic model was used to simulate the biomass growth considering a Monod-type relation to include the effect of oxygen concentration. The model considered the description of: temperature and oxygen concentration profiles in the gas phase and temperature and oxygen, biomass, and substrate concentration profiles in the solid–liquid phase. These profiles were described as a function of time considering also radial and axial variations.

The model predictions were in accordance with results reported in the literature for composting processes. The model was used to determine the effect of the design variables with the next general results: use a wide bioreactor, the initial substrate concentration has to be enough for biomass growth and the initial biomass concentration should be small for a fixed initial substrate concentration, the bioreactor insulation is critical, and the length of the bioreactor as well as the interstitial velocity of the fed air are not significant under the studied conditions. This holds true if a high value of logarithmic decimal reduction is pursued.

A sensitivity analysis allows determining the parameters that influence the most the predicted concentration and temperature profiles, especially in the maximum temperature that can be attained in the solid–liquid phase and the length of high temperature conditions.

Conflict of interest

The authors declare that they have no conflict of interest.

Acknowledgement

OGO acknowledges funding from FAI (C15-FAI-04-35.35).

References

Ahn, H., Sauer, T.J., Richard, T.L., Glanville, T.D., 2009. Determination of thermal properties of composting bulking materials. Bioresour. Technol. 100, 3974–3981.

Annan, J.S., White, R.K., 1998. Evaluation of techniques for measuring air filled porosity in composts of municipal biosolids and wood chips. In: Das, K.C., Graves, E.F. (Eds.), Composting in the Southeast. The University of Georgia, USA.

Bari, Q.H., Koenig, A., Guide, T., 2000. Kinetic analysis of forced aeration composting—I. Reaction rates and temperature. Waste Manage. Res. 18, 303–312.

Bergman, T.L., Lavine, A.S., Incropera, F.P., Dewitt, D.P., 2011. Fundamentals of Heat and Mass Transfer, seventh ed. John Wiley & Sons, USA.

Bongochgetsakul, N., Ishida, T., 2008. A new analytical approach to optimizing the design of large-scale composting systems. Bioresour. Technol. 99, 1630–1641.

Briski, F., Horgas, N., Vukovic, M., Gomzi, Z., 2003. Aerobic composting of tobacco industry solid waste—simulation of the process. Clean Technol. Environ. Policy 5, 295–301.

Churchill, S.W., Chu, H.H.S., 1975. Correlating equations for laminar and turbulent free convection from a vertical plate. Int. J. Heat Mass Transf. 18, 1323–1329.

Contois, D.E., 1959. Kinetics of bacterial growth: relationship between population density and specific growth rate of continuous cultures. J. Gen. Microbiol. 21, 40–50.

Cornell Waste Management Institute, 1996. Calculating the Oxygen Diffusion Coefficient in Air, http://compost.css.cornell.edu/oxygen/oxygen.diff.air.html#txt. (Accessed 19 February 2016).

Davis, M.E., 1984. Numerical Methods and Modeling for Chemical Engineers. John Wiley & Sons, New York.

Delgado, J.M.P.Q., 2007. Longitudinal and transverse dispersion in porous media. Chem. Eng. Res. Des. 85, 1245–1252.

Diaz, L.F., Savage, G.M., 2007. Factors that affect the process. In: Diaz, L.F., de Bertoldi, M., Bidlingmaier, W., Stentiford, E. (Eds.), Compost Science and Technology. Elsevier, The Netherlands, pp. 49–65.

Fuchs, J.G., 2010. Interactions between beneficial and harmful microorganisms: From the composting process to compost application. In: Insam, H., Franke-Whittle, I., Goberna, M. (Eds.), Microbes at Work. Springer, New York, pp. 213–229.

Ge, J., Huang, G., Huang, J., Zeng, J., Han, L., 2015. Modeling of oxygen uptake rate evolution in pig manure-wheat straw aerobic composting process. Chem. Eng. J. 276, 29–36.

Gea, T., Barrena, R., Artola, A., Sanchez, A., 2007. Optimal bulking agent particle size and usage for heat retention and disinfection in domestic wastewater sludge composting. Waste Manage. 27, 1108–1116.

Hamelers, H.V.M., 2001. A Mathematical Model for Composting Kinetics. Doctoral Dissertation. Wageningen University.

Hamelers, H.V.M., 2004. Modeling composting kinetics: a review of approaches. Rev. Environ. Sci. Bio/Technol. 3, 331–342.

Haug, R.T., 1993. The Practical Handbook of Compost Engineering. Lewis Publishers, Florida.

Higgins, C.W., Walker, L.P., 2003. Validation of a new model for aerobic organic solids decomposition: simulations with substrate specific kinetics. Process Biochem. 36, 875–884.
Insam, H., de Bertoldi, M., 2007. Microbiology of the composting process. In: Diaz, L.F., de Bertoldi, M., Bidlingmaier, W., Stentiford, E. (Eds.), Compost Science and Technology. Elsevier, The Netherlands, pp. 25–48.
Kiyasudeen, S.K., Ibrahim, M.H., Quaik, S., Ismail, A.S., 2016. Prospects of Organic Waste Management and the Significance of Earthworms. Springer, Switzerland.
Krupiczka, R., 1967. Analysis of thermal conductivity in granular materials. Int. J. Chem. Eng. 7, 22–144.
Kulcu, R., Yaldiz, O., 2004. Determination of aeration rate and kinetics of composting some agricultural wastes. Bioresour. Technol. 93, 49–57.
Lashermes, G., Zhang, Y., Houot, S., Steyer, J.P., Patureau, D., Barriuso, E., Garnier, P., 2013. Simulation of organic matter and pollutant evolution during composting: the COP-compost model. J. Environ. Qual. 42, 361–372.
Lin, Y.P., Huang, G.H., Lu, H.W., He, L., 2008. Modeling of substrate degradation and oxygen consumption in waste composting processes. Waste Manage. 28, 1375–1385.
Mason, I.G., 2006. Mathematical modelling of the composting process: a review. Waste Manage. 26, 3–21.
McKinley, V.L., Vestal, J.R., 1984. Biokinetic analyses of adaptation and succession: microbial activity in composting municipal sewage sludge. Appl. Environ. Microbiol. 47, 933–941.
Mohee, R., White, R.K., Das, K.C., 1998. Simulation model for composting cellulosic (bagasse) substrates. Compost Sci. Util. 6, 82–92.
Monod, J., 1949. The growth of bacterial cultures. Ann. Rev. Microbiol. 3, 371–394.
Nakayama, A., Kuwahara, F., Sano, Y., Nakasaki, K., Fukazawa, T., 2007a. A numerical modeling of composting process with aeration. Proc. 2nd Int. Conf. Porous Media Appl. Sci. Eng., 17–21.
Nakayama, A., Nakasaki, K., Kuwahara, F., Sano, Y., 2007b. A lumped parameter heat transfer analysis for composting processes with aeration. Trans. ASME 129, 902–906.
Petric, I., Mustafic, N., 2015. Dynamic modeling the composting process of the mixture of poultry manure and wheat straw. J. Environ. Manage. 161, 392–401.
Petric, I., Selimbasic, V., 2008a. Composting of poultry manure and wheat straw in a closed reactor: optimum mixture ratio and evolution of parameters. Biodegradation 19, 53–63.
Petric, I., Selimbasic, V., 2008b. Development and validation of mathematical model for aerobic composting process. Chem. Eng. J. 139, 304–317.
Qin, X., Huang, G., Zeng, G., Chakma, A., Xi, B., 2007. A fuzzy composting process model. Air Waste Manage. Assoc. 57, 535–550.
Richard, T.L., Walker, L.P., Gossett, J.M., 2006. Effects of oxygen on aerobic solid-state biodegradation kinetics. Biotechnol. Prog. 22, 60–69.
Rosso, L., Lobry, J.R., Flandrois, J.P., 1993. An unexpected correlation between cardinal temperatures of microbial growth highlighted by a new model. J. Theor. Biol. 162, 447–463.
Sahraoui, M., Kaviany, M., Marshall, H., 1990. Natural convection from horizontal disks and rings. Trans. ASME 112, 110–116.
Sander, R., 2015. Compilation of Henry's law constants (version 4.0) for water as solvent. Atmos. Chem. Phys. 15, 4399–4981.
Shishido, T., Seki, H., 2015. Laboratory-scale experiment for an active-stage composting process under the same material and operating conditions. J. Agric. Meteorol. 71, 111–123.
Sole-Mauri, F., Illa, J., Magri, A., Prenafeta-Boldu, F.X., Flotats, X., 2007. An integrated biochemical and physical model for the composting process. Bioresour. Technol. 98, 3278–3293.
Tremier, A., de Guardia, A., Massiani, C., Paul, E., Martel, J.L., 2005. A respirometric method for characterising the organic composition and biodegradation kinetics and the temperature influence on the biodegradation kinetics, for a mixture of sludge and bulking agent to be co-composted. Bioresour. Technol. 96, 169–180.
VanderGheynst, J.S., Gossett, J.M., Walker, L.P., 1997. High-solids aerobic decomposition: pilot-scale reactor development and experimentation. Process Biochem. 32, 361–375.
Vasiliadou, I.A., Chowdhury, A.K., Akratos, C.S., Tekerlekopoulou, A.G., Pavlou, S., Vayenas, D.V., 2015. Mathematical modeling of olive mill waste composting process. Waste Manage. 43, 61–71.
Wang, Z., Li, Y., 2014. A theoretical derivation of the Contois equation for kinetic modeling of the microbial degradation on insoluble substrates. Biochem. Eng. J. 82, 134–138.
Weppen, P., 2001. Process calorimetry on composting of municipal organic wastes. Biomass Bioenergy 21, 289–299.
Zambra, C.E., Moraga, N.O., Escudey, M., 2011. Heat and mass transfer in unsaturated porous media: moisture effects in compost piles self-heating. Int. J. Heat Mass Transf. 54, 2801–2810.